# Stochastic-Chebyshev-expansion approach for the simulation of linear polariton spectroscopy in the collective-coupling regime

Braden M. Weight [1,*] and Pengfei Huo [2,3,4,†]

[1]*Department of Physics and Astronomy, University of Rochester, Rochester, New York 14627, USA*
[2]*Department of Chemistry, University of Rochester, 120 Trustee Road, Rochester, New York 14627, USA*
[3]*The Institute of Optics, Hajim School of Engineering, University of Rochester, Rochester, New York 14627, USA*
[4]*Center for Coherence and Quantum Science, University of Rochester, Rochester, New York 14627, USA*

Molecular polaritons are becoming one of the leading directions to control a multitude of chemical and physical processes, such as charge transfer, selective bond breaking, and excited-state dynamics. Accurately and efficiently simulating polariton properties under the collective-coupling regimes (between $N$ molecules and the cavity mode) remains a central theoretical challenge. In this work, we use a stochastic resolution of the identity approach coupled with a Chebyshev expansion to compute various polariton photophysical properties, with a substantially reduced computational effort than would be needed for a direct diagonalization of the same Hamiltonian, which is often the bottleneck for such large dimensionality. Such quantities of interest are the total density of states (the eigenspectrum of the Hamiltonian) and the transmission spectrum (a probe of the photonic degrees of freedom), the latter of which is a direct observable in the experiment. We simulate the linear spectroscopy of molecule-cavity hybrid systems, specifically exploring the effects of the distribution and magnitude of molecular disorder for one, few, and many coupled molecules. We compare our numerical results to recent work, which formulated analytic expressions in the large-$N$ limit for the spectroscopic signals. We find that our results match those of the analytic results when $N = 100$, at which point we find that the collective effects for linear spectroscopy are converged.

## I. INTRODUCTION

Exciton polaritons, light-matter hybrid states with cavity photon frequencies in the eV range, have recently become a topic of great interest for their ability to alter both chemical reactions/properties in the ground [1–9] and excited [3,10–15] states as well as photophysics/spectroscopies [3,16–34] such as quasiparticle propagation [35–41]. Much theoretical work has been performed to simulate these intrinsically many-body systems [8,9,15,42–51]. An exciton polariton is an entangled state of light and matter in which the native excitonic and photonic degrees of freedom hybridize to form new states. These new states can be tuned in various ways to modify chemical and physical properties, such as the potential energy landscape or the emission efficiency of materials. However, much is still unknown about these new hybrid states. For example, collective effects—which arise from the coherent coupling of $N = 2\text{-}10^{10}$ molecules to a single optical cavity mode—are largely unexplored due to the size complexity of the light-matter Hamiltonian.

To understand all of these effects, one turns to various types of spectra to decipher how the molecular and photonic degrees of freedom (DOFs) are coupled to each other and their surroundings. The simplest realization of this is the linear spectroscopy in which the system encounters a measurement photon at some frequency $\omega$. For the molecule-cavity hybrid system, there are multiple types of linear spectroscopy that can be performed: (i) reflectance, (ii) absorption, and (iii) transmission. In the experiment, the reflectance $R$ and transmission $T$ spectroscopies are collected directly. The absorption $A$ is then calculated as $A\% = 1 - T\% - R\%$ as an indirect measurement. Our focus here is the transmission spectroscopy whose intensity is proportional to the photon number inside the cavity, $T \propto \langle \hat{a}^\dagger \hat{a} \rangle$ [52,53].

Numerous theoretical and experimental works have explored the effects of collectivity on linear spectroscopy [13,15,24,25,29,54–58]. However, many of these works have assumed that the collective nature of the spectral signatures requires a large number of molecules $N$, such as those analytical works relying on thermodynamic limits of linear response equations, single-particle Green's functions, and molecular susceptibilities, etc. [29,54]. Therefore, it is widely assumed that the collective nature of these hybrid systems is not directly reachable with standard "brute force"-style diagonalization techniques.

In this work, we directly simulate the transmission spectroscopy of coupled light-matter systems, forming exciton polaritons, in the presence of various molecular excitation frequency disorders. We find that the transmission spectra take on drastically varied characteristics between different electronic disorder types (Gaussian, rectangular, Lorentzian) as well as between one-, two-, and many-molecule (more than

---

*Contact author: bweight@ur.rochester.edu
†Contact author: pengfei.huo@rochester.edu

100) systems for a given disorder type. Second, the Lorentzian profile shows little-to-no modifications by varying $N$. Finally, our simulations reveal that the number of molecules necessary to saturate the collective effects for linear transmission spectroscopy to be $N \sim 100$ or less, irrespective of the disorder type and magnitude.

## II. LIGHT-MATTER HAMILTONIAN

In this work, we are interested in exciton polaritons [15,47], which are composed of electronic excitations (typically in the frequency regime of $\sim$1–5 eV) coupled to a photonic excitation of similar frequency. Moreover, we focus on collections of excitons that simultaneously couple to one photonic mode to explore the resulting linear spectroscopies in the presence of static excitonic disorder of varying magnitude.

The nonrelativistic Pauli-Fierz Hamiltonian $\hat{H}_{PF}$ has been widely applied [15,45,47,59–62] to study light-matter hybrid systems. A widely used approximation to the Pauli-Fierz Hamiltonian for many molecules in the weak-to-strong-coupling regime is the Tavis-Cummings (TC) Hamiltonian $\hat{H}_{TC}$ [63–66]. The TC Hamiltonian simultaneously drops the dipole self-energy (DSE) and introduces the rotating-wave approximation (RWA). The TC Hamiltonian can be written as

$$\hat{H}_{TC} = \hat{H}_{el} + \hat{H}_{ph} + \hat{H}_{el-ph}, \tag{1a}$$

$$\hat{H}_{el} = \sum_A^N \left( \bigotimes_{B<A}^N \hat{\mathbb{1}}_{el}^{(B)} \otimes \hat{H}_{el}^{(A)} \otimes \bigotimes_{B>A}^N \hat{\mathbb{1}}_{el}^{(B)} \right) \otimes \hat{\mathbb{1}}_{ph}, \tag{1b}$$

$$\hat{H}_{ph} = \left( \bigotimes_A^N \hat{\mathbb{1}}_{el}^{(A)} \right) \otimes \omega_c \hat{a}^\dagger \hat{a}, \tag{1c}$$

$$\hat{H}_{el-ph} = \omega_c A_0 \sum_A^N \left( \bigotimes_{B<A}^N \hat{\mathbb{1}}_{el}^{(B)} \otimes \hat{\mu}^{(A)} \otimes \bigotimes_{B>A}^N \hat{\mathbb{1}}_{el}^{(B)} \right)$$
$$\otimes (\hat{a}^\dagger + \hat{a}), \tag{1d}$$

where $\hat{\mu} \equiv \vec{\mu} \cdot \vec{e}$ is the molecular dipole operator projected into the photonic polarization direction. Here, $\omega_c$ is the cavity frequency and

$$A_0 = \sqrt{\frac{1}{2\omega_c \epsilon \mathcal{V}}} \tag{2}$$

is the light-matter coupling strength with $\mathcal{V}$ as the cavity mode volume and $\epsilon$ as the dielectric constant of the medium.

The exact solution of the above Hamiltonian using the complete Hilbert space is already intractable for more than $N = 10$–20 molecules. This is because the dimension of the Hamiltonian scales exponentially with the number of molecules as $\dim[\hat{H}_{TC}] \propto 2^N$, assuming that the molecular degrees of freedom (DOFs) have only two basis states, $\{|g\rangle, |e\rangle\}$. However, since we are interested in collective effects, we will restrict the description of the above Hamiltonian to the basis of the first-excited subspace. In the singly excited subspace, the dimension scales as $\dim[\hat{H}_{TC}] \propto N$ [8].

For clarity, the zero- ($|\mathcal{S}_0\rangle$) and single-excitation ($|\mathcal{S}_1\rangle$) subspaces including only $|g\rangle$ and $|e\rangle$ electronic states, i.e., first two eigenstates of $\hat{H}_{el}$ (extension to multiple electronically

excited states and an *ab initio* molecular system to come in forthcoming work), for each molecule,

$$|\mathcal{S}_0\rangle = \bigotimes_A^N |g\rangle^{(A)} \otimes |0\rangle, \tag{3a}$$

$$|\mathcal{S}_1\rangle = \sum_A^N \left( \bigotimes_{B<A}^N |g\rangle^{(B)} \otimes |e\rangle^{(A)} \otimes \bigotimes_{B>A}^N |g\rangle^{(B)} \right) \otimes |0\rangle$$
$$+ \bigotimes_A^N |g\rangle^{(A)} \otimes |1\rangle. \tag{3b}$$

We further make the assumption that there are no permanent electronic dipoles, thus decoupling the collective ground state, $\langle g, \ldots, g, 0|\omega A_0 \hat{\mu}(\hat{a}^\dagger + \hat{a})|g, \ldots, g, 1\rangle = \omega A_0 \sum_A^N \mu_{00}^{(A)} = 0$. Alternatively, to achieve the identical result, we could work in the coherent-state basis [67,68], which shifts away a constant proportional to the identity in the electronic subspace from the Hamiltonian whereby $\hat{\mu} \to \hat{\mu} - \langle \mu \rangle$ where $\langle \mu \rangle \equiv \langle \mathcal{S}_0 | \hat{\mu} | \mathcal{S}_0 \rangle$ is chosen to be the ground-state permanent dipole moment. In both situations, the ground state is decoupled from the light-matter interaction in the TC Hamiltonian, which is valid below the ultrastrong-coupling regime where most experiments in linear spectroscopies of polaritons reside [69]. In this case, the TC Hamiltonian, without the collective ground state $|\mathcal{S}_0\rangle$, which is to say, $|\mathcal{S}_1\rangle\langle\mathcal{S}_1|\hat{H}_{JC}|\mathcal{S}_1\rangle\langle\mathcal{S}_1|$, can be written as

$$\hat{H}_{TC} \doteq \begin{bmatrix} E_{eg}^{(0)} & 0 & 0 & \cdots & \omega_c A_0 \mu_{eg}^{(0)} \\ 0 & E_{eg}^{(1)} & 0 & \cdots & \omega_c A_0 \mu_{eg}^{(1)} \\ 0 & 0 & E_{eg}^{(2)} & \cdots & \omega_c A_0 \mu_{eg}^{(2)} \\ \vdots & \vdots & \vdots & \ddots & \vdots \\ \omega_c A_0 \mu_{eg}^{(0)} & \omega_c A_0 \mu_{eg}^{(1)} & \omega_c A_0 \mu_{eg}^{(2)} & \cdots & \omega_c \end{bmatrix}. \tag{4}$$

Here, $E_{eg}^{(A)} = E_e^{(A)} - E_g^{(A)}$ is the ground-to-excited transition energy of molecule $A$ with associated ground-to-excited transition dipole moment $\mu_{eg}^{(A)} = \vec{\mu}_{eg}^{(A)} \cdot \vec{e}$.

For convenience of notation, we define the collective-coupling strength as

$$\tilde{A}_0 = A_0 \sqrt{N}. \tag{5}$$

The use of this parameter fixes the collective Rabi splitting $\Omega_R$ for any number of molecules $N$ since $\Omega_R \propto A_0 \sqrt{N}$ for $N$ molecules resonantly coupled to the cavity. For all simulations of the current work, we restrict the cavity parameters to $\tilde{A}_0 = 0.01$ a.u., $\omega_c = 1.00$ a.u., $\langle E_{eg} \rangle_N = 1.00$ a.u., and $\mu_{eg}^{(A)} = 1.00$ a.u. In this case, the average of the molecular transition frequencies are resonant with the cavity frequency, $\langle \Delta E_{eg} \rangle_N = \omega_c = 1.00$, and all molecular dipole moments are fixed and equal. As an example, for $N = 3$ and the above parameters, the working Hamiltonian becomes

$$\hat{H}_{TC} \doteq \begin{bmatrix} E_{eg}^{(0)} & 0 & 0 & 0.01/\sqrt{3} \\ 0 & E_{eg}^{(1)} & 0 & 0.01/\sqrt{3} \\ 0 & 0 & E_{eg}^{(2)} & 0.01/\sqrt{3} \\ 0.01/\sqrt{3} & 0.01/\sqrt{3} & 0.01/\sqrt{3} & 1 \end{bmatrix}.$$

As we will see later, the transition frequencies of the molecular DOFs, $\Delta E_{eg}$, will be sampled from various distributions, Gaussian, rectangular, and Lorentzian, which represent the primary results of this work. Also, the high degree of symmetry and sparsity in this Hamiltonian lends itself well to approximate approaches that depend on the efficient implementation of matrix-vector multiplication discussed in the following section [28,63,70].

The definition of strong coupling arises through the definition of a unitless coupling parameter $\eta = \Omega_R/(2\omega_c)$ (with $\omega_c = 1.0$ a.u. in this work). For a set of identical molecules perfectly resonant with the cavity, strong coupling is defined as $\eta = \Omega_R/2 = 0.01$, ultrastrong coupling as $\eta = \Omega_R/2 = 0.1$, and deep-strong coupling as $\eta = \Omega_R/2 = 1.0$. Note that the Rabi splitting depends on the molecular disorder, $\Omega_R \equiv \Omega_R(\frac{\sigma}{\tilde{A}_0})$. In the present work, at $\sigma/\tilde{A}_0 = 0.0$ (no molecular disorder), $\eta = \Omega_R/2 = \tilde{A}_0 = 0.01$ for all cases in all figures. This indicates that the system is initially at the boundary between the weak- and strong-coupling regimes. We note that the results presented in this work are independent of the regime at zero disorder since all conclusions only depend on the ratio of the disorder to the Rabi splitting at zero disorder $\sim \sigma/\tilde{A}_0$.

### III. STOCHASTIC-CHEBYSHEV APPROACH

In this work, we aim to simulate a partial density of states (DOS) for a given Hamiltonian. Following closely the notation of Ref. [28], the total density operator is defined as

$$\text{DOS}(E) = \text{Tr}[\hat{\delta}(E - \hat{H})] = \sum_i \delta(E - E_i), \qquad (6)$$

where $E$ is an arbitrary energy, Tr is the trace operation, $\hat{H}$ is an arbitrary Hamiltonian, $E_i$ is the $i$th eigenvalue of the Hamiltonian $\hat{H}$, and $\delta$ is the standard Dirac $\delta$ function. In practice, if one cannot directly diagonalize the Hamiltonian, it is hard to know the set of $E_i$ to generate the exact DOS. However, in the following, we will both approximate the $\delta$ function and obtain the DOS without diagonalizing the Hamiltonian or knowing its eigenvalues [28,71]. The code and data that support the findings of this article are openly available [72].

#### A. Chebyshev expansion of an operator function

The $\delta$ function of an operator can be approximated as various different functions in the limit of infinitely small broadening parameter $\gamma$. Here, we choose a $\delta$ Gaussian as

$$\delta(\hat{H} - E) = \lim_{\gamma \to 0} \frac{e^{-\frac{(\hat{H}-E)^2}{2\gamma^2}}}{\gamma\sqrt{2\pi}}, \qquad (7)$$

though other functions can be used, such as a Lorentzian $\sim \gamma/(\hat{H}^2 + \gamma^2)$. The Chebyshev polynomial expansion of an operator function can be written as

$$\delta(\hat{H} - E)|\lambda\rangle = \sum_{l=1}^{\infty} c_l(E, \gamma)\hat{T}_l(\hat{\bar{H}})|\lambda_{l-1}\rangle$$

$$\approx \sum_{l=0}^{N_{\text{Cheb}}} c_l(E, \gamma)|\lambda_l(\hat{\bar{H}})\rangle, \qquad (8)$$

where $c_l(E, \gamma)$ are the expansion coefficients, which encode the finite-width spectral function and the energy grid point, $E$, on which it is evaluated. In practice, the infinite sum over Chebyshev moments is truncated to $N_{\text{Cheb}}$ terms, which is treated as a convergence parameter. The action of $\hat{T}_l(\hat{\bar{H}})$ on an arbitrary vector $|\lambda\rangle$ is defined as $\hat{T}_l(\hat{\bar{H}})|\lambda_{l-1}\rangle = |\lambda_l(\hat{\bar{H}})\rangle$. The coefficients are evaluated by the discrete Fourier transform as

$$c_l(E, \gamma) = (2 - \delta_{l,0}) \int_0^{2\pi} d\theta F(\theta; E)e^{il\theta}, \qquad (9)$$

with $F(\theta; E)$ dependent on the broadening function as

$$F(\theta; E) = \frac{1}{\gamma\sqrt{2\pi}} e^{\frac{[\Delta E \cos(\theta) - (E-\bar{E})]^2}{2\gamma^2}}. \qquad (10)$$

These coefficients $c_l(E, \gamma)$ can be evaluated once and stored on disk for all calculations which share the same number of Chebyshev moments $N_{\text{Cheb}}$, window size $\Delta E$ (defined below), finite broadening $\gamma$, and energy grid points $E$. All simulations performed in this work share the same Chebyshev coefficients $c_l(E, \gamma)$ since all such parameters are fixed.

The recursion relation of Chebyshev vectors can be written as

$$|\lambda_0\rangle = |\lambda\rangle, \qquad (11a)$$

$$|\lambda_1(\hat{\bar{H}})\rangle = \hat{\bar{H}}|\lambda_0\rangle, \qquad (11b)$$

$$|\lambda_l(\hat{\bar{H}})\rangle = 2\hat{\bar{H}}|\lambda_{l-1}(\hat{\bar{H}})\rangle - |\lambda_{l-2}(\hat{\bar{H}})\rangle. \qquad (11c)$$

Since the Chebyshev series is only defined on the interval $(-1, 1)$, the shifted and normalized Hamiltonian is

$$\hat{\bar{H}} = \frac{\hat{H} - \bar{E}\hat{\mathbb{1}}}{\Delta E}, \qquad (12)$$

where $\bar{E} = \omega_c = \langle E_{eg}\rangle_N = 1.00$ is the expected average of the spectrum and $\Delta E/\tilde{A}_0 = 64 = 4\,\sigma^{\max}/\tilde{A}_0$ ($\sigma$ to be introduced later) is the expected span of the spectrum such that the eigenvalues of $\hat{\bar{H}}$ lie on the interval $(-1, 1)$.

#### B. Trace of an operator in a stochastic basis

Using the stochastic resolution of the identity, $\mathbb{1} = \langle|\xi\rangle\langle\xi|\rangle_\xi$, the trace can be written as

$$\text{Tr}[\delta(\hat{H} - E)] = \langle\langle\xi|\delta(\hat{H} - E)|\xi\rangle\rangle_\xi$$

$$= \frac{1}{N_r}\sum_r^{N_r}\langle\xi_r|\delta(\hat{H} - E)|\xi_r\rangle, \qquad (13)$$

where $|\xi_r\rangle$ is a random vector of size $N = \dim(\hat{H})$ with elements $\langle n|\xi_r\rangle = e^{i\theta}$ where $\theta \in [0, 2\pi)$. The statistics satisfy $\langle\langle\xi_r|\xi_{r'}\rangle\rangle_\xi = \delta_{rr'}$, and $\langle\cdots\rangle_\xi$ indicates a classical arithmetic average over the $N_r$ random vectors $\{|\xi_r\rangle\}$.

#### C. Density of states

Combining the Chebyshev expansion with the stochastic trace, we can write down the approximate DOS for a Hamiltonian. The stochastic-Chebyshev approach to calculating the
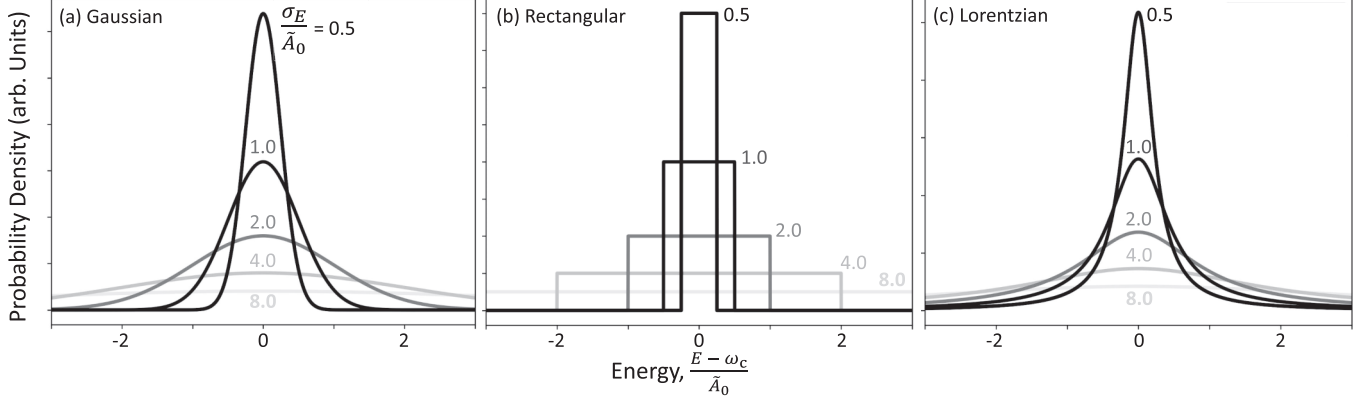
FIG. 1. (a) Gaussian, (b) rectangular, and (c) Lorentzian distributions for the molecular excitation frequencies $E_{eg}^{(A)}$. The shade of gray indicates the varying magnitudes of disorder $\sigma/\tilde{A}_0$ relative to the collective-coupling strength $\tilde{A}_0$ (dark for weak disorder, light for strong disorder).

DOS can then be compactly written as

$$\text{DOS}(E, \gamma) = \text{Tr}[\delta(\hat{H} - E)]$$

$$\approx \frac{1}{N_r} \sum_r^{N_r} \langle \xi_r | e^{-\frac{(\hat{H}-E)^2}{2\gamma^2}} | \xi_r \rangle$$

$$\approx \frac{1}{N_r} \sum_r^{N_r} \sum_{l=0}^{N_{\text{Cheb}}} c_l(E, \gamma) \langle \xi_r | \xi_{rl}(\hat{\tilde{H}}) \rangle \qquad (14)$$

where $N_{\text{Cheb}}$ is the number of polynomials in the truncated Chebyshev expansion (treated as a convergence parameter). This parameter scales as $N_{\text{Cheb}} \propto \frac{\Delta E}{\gamma}$, where $\Delta E$ is the energy scale of the eigenvalues [Eq. (12)] and $\gamma$ is the finite-width $\delta$-broadening parameter [Eq. (7)].

### D. Transmission spectrum

The stochastic-Chebyshev photon transmission spectrum (TM), which is proportional to the photonic DOS, can be computed similarly as

$$\text{TM}(E, \gamma) \propto \text{DOS}_{\text{ph}}(E, \gamma) = \text{Tr}[\hat{P}_{\text{ph}} \delta(\hat{H} - E)]$$

$$\approx \frac{1}{N_r} \sum_r^{N_r} \sum_{l=0}^{N_{\text{Cheb}}} c_l(E, \gamma) \langle \xi_r | \hat{P}_{\text{ph}} | \xi_{rl}(\hat{\tilde{H}}) \rangle, \qquad (15)$$

where $\hat{P}_{\text{ph}} = |g, \ldots, g, 1\rangle\langle g, \ldots, g, 1|$ is the projection operator which picks out the excited photon basis element. Equation (15) compactly represents the primary quantity used in this work [72].

## IV. MODEL SYSTEMS AND COMPUTATIONAL DETAILS

In the experiment, the molecular DOFs always have some form of intrinsic disorder (energetic disorder or orientation of the dipole relative to the cavity field intensity or the transition dipole strength). Molecular disorder can arise from various phenomena, including both internal (e.g., vibrational modes of the molecule) and external (e.g., interactions with a solvent) DOFs. Furthermore, there are two main categories of disorder: (I) dynamic disorder (e.g., thermal fluctuations from vibrations—internal and/or external), which manifests as a

broadening of the transition energy/spectrum, and (II) static disorder (e.g., molecular defects, reactant/product species, isomers, inhomogeneous sizes of particles such as quantum dots or nanoplatelets, varied external environments of the molecules, multiple electronic states per molecule, etc.), which may provide multiple spectral peaks [73].

In the present work, we consider three distributions of molecule excitation frequencies as shown in Fig. 1: (i) Gaussian, (ii) rectangular, and (iii) Lorentzian. Thus, we focus on the role of strong disorder in the molecular sample. Specifically, we consider the probability distributions: Gaussian,

$$\mathcal{P}^{\text{G}}(E - \bar{E}) = \frac{1}{\sqrt{2\pi} \, \sigma} e^{-\frac{E-\bar{E}}{2\sigma^2}}, \qquad (16)$$

rectangular,

$$\mathcal{P}^{\text{R}}(E - \bar{E}) = \begin{cases} \frac{1}{\sigma}, & |E - \bar{E}| \leqslant \frac{\sigma}{2}, \\ 0, & \text{else}, \end{cases} \qquad (17)$$

and Lorentzian,

$$\mathcal{P}^{\text{L}}(E - \bar{E}) = \frac{1}{\pi} \frac{\sigma}{(E - \bar{E})^2 + \sigma^2}. \qquad (18)$$

These disorder distributions were previously explored with analytic linear response models under a large-$N$ expansion in Ref. [29]. The rectangular distribution can be considered as a limiting case of a uniform static disorder where, for example, inhomogeneous particle sizes (e.g., quantum dots) can lead to equally distributed features in the frequency domain [73]. We expect that the Gaussian distribution, in the absence of *a priori* static disorder, will be the most prevalent in the experiment due to the random fluctuations (i.e., high-frequency, Markovian noise) of the solvent DOFs ubiquitous in most experimental conditions. Of course, the true shape of the excitation spectra will also depend on the electronic structure of the molecules themselves. Formally, the stochastic error scales as $O(1/\sqrt{NN_r})$, where $N_r$ is the number of random vectors used in the stochastic average and $N$ is the dimension of the Hamiltonian $\hat{H}$ (i.e., the number of molecules in the current context). However, we find that the error in the partial density of states scales unfavorably with the number of molecules due to the small dimension of the
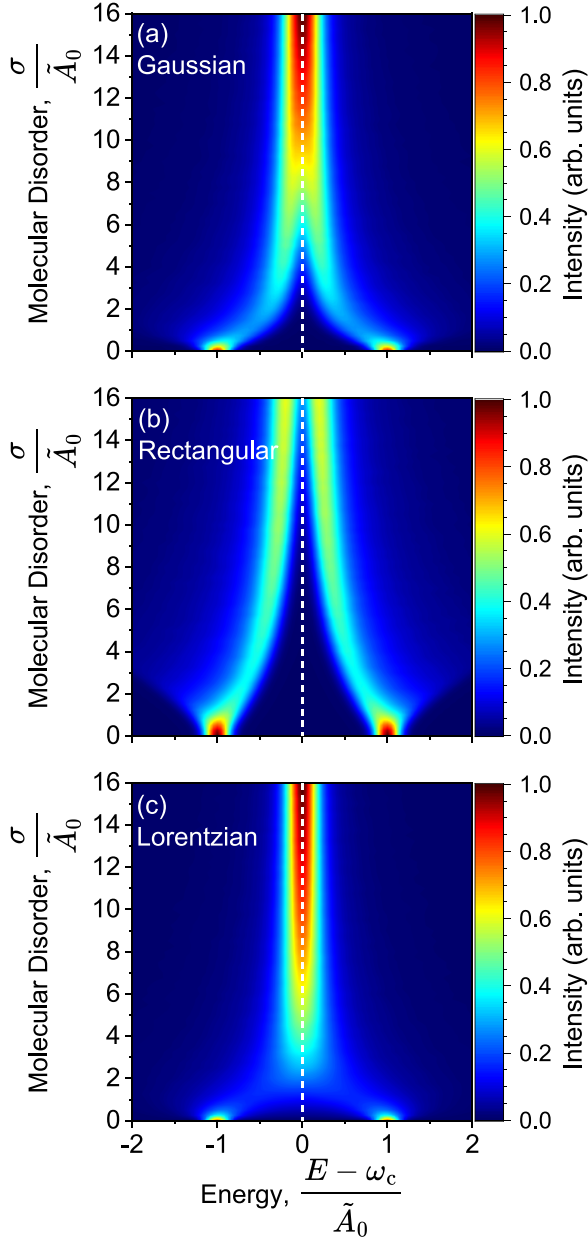
FIG. 2. Transmission spectra for $N = 1$ at varying magnitude of energetic disorders (vertical axis) of the molecules with widths $\sigma$ with distribution (a) Gaussian, (b) rectangular, and (c) Lorentzian. $A_0 = 0.01$ a.u., $\omega_c = 1.00$ a.u., $N_r = 50\,000$, $N_{\text{Cheb}} = 2500$, $\gamma = 0.001$ a.u.

FIG. 3. Transmission spectra for $N = 1$ at varying Gaussian energetic disorders (vertical axis) of the molecules with widths $\sigma$ with distribution (a) Gaussian, (b) rectangular, and (c) Lorentzian. $A_0 = 0.01$ a.u., $\omega_c = 1.00$ a.u., $N_r = 50\,000$, $N_{\text{Cheb}} = 2500$, $\gamma = 0.001$ a.u. Note that the data shown here are identical to Fig. 2 except that the intensity is on a log scale.

projection operator $(\dim[\hat{P}_{\text{ph}}]/\dim[\hat{H}] \sim 1/N \ll 1)$ and due to the presence of disorder removing beneficial symmetry from the Hamiltonian. Thus, in practice, we use $N_r = 50\,000$ random vectors in all calculations to ensure convergence and consistency. Unless otherwise stated, we use $\gamma = \tilde{A}_0/10 = 0.001$ a.u., $\Delta E = 0.640$ a.u., and $N_{\text{Cheb}} = 2500$ with a ratio $\frac{\Delta E}{\gamma} = 640$. Figures 2–9 present the transmission spectra for each disorder type [panels, Eqs. (16)–(18)] as functions of the disorder in the molecular transition frequencies $\sigma$ (vertical axis) for (Fig. 2) $N = 1$, (Fig. 4) $N = 2$, (Fig. 6) $N = 100$, and (Fig. 8) $N = 1000$ molecules. Figures 3, 5, 7, 9 are the log-scale intensity analogs to Figs. 2, 4, 6, 8.
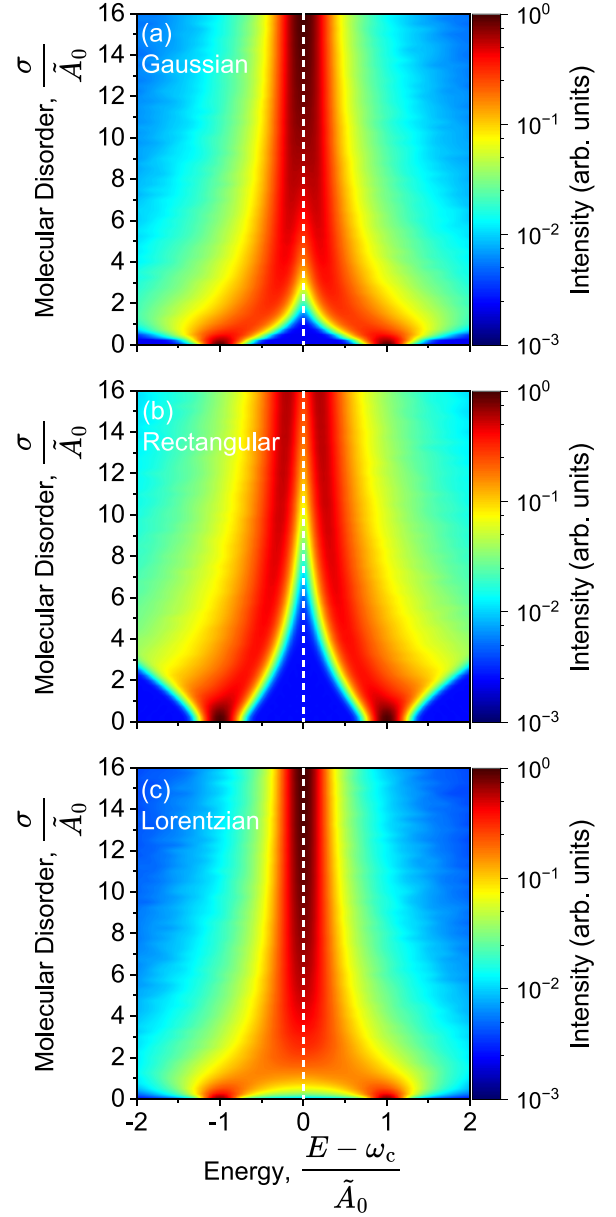
The scaling of this approach can be written as $O(N_r N_{\text{Cheb}} d^2)$ rather than $O(d^3)$ for direct diagonalization. Since the Hamiltonian is sparse, the final scaling of the stochastic-Chebyshev is $O(N_r N_{\text{Cheb}} d)$, linear in the dimension of the Hilbert space $d \equiv \dim[\hat{H}]$.

## V. RESULTS AND DISCUSSION

Starting with $N = 1$ under Gaussian disorder in Fig. 2(a), we find that that the upper (UP) and lower polariton (LP) spectral bands collapse (decrease in Rabi splitting, $\Omega_R = E_{\text{UP}} - E_{\text{LP}}$) nonlinearly with an increasing energetic disorder
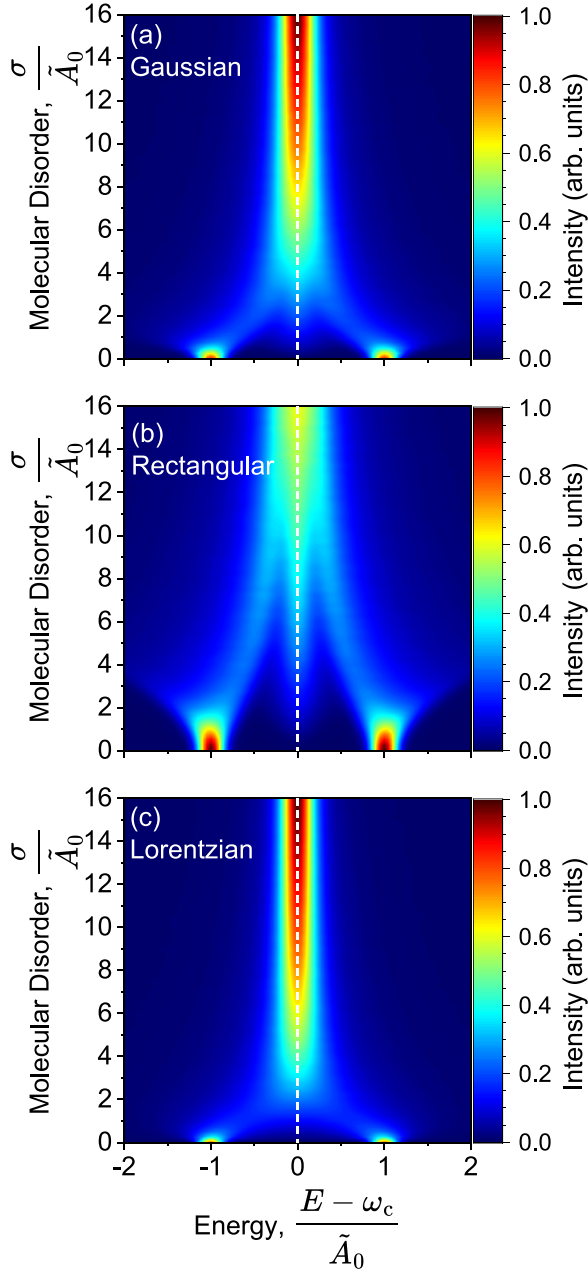
FIG. 4. Transmission spectra for $N = 2$ at varying magnitude of energetic disorders (vertical axis) of the molecules with widths $\sigma$ with distribution (a) Gaussian, (b) rectangular, and (c) Lorentzian. $A_0 = 0.01$ a.u., $\omega_c = 1.00$ a.u., $N_r = 50\,000$, $N_{\text{Cheb}} = 2500$, $\gamma = 0.001$ a.u.



FIG. 5. Transmission spectra for $N = 2$ at varying Gaussian energetic disorders (vertical axis) of the molecules with widths $\sigma$ with distribution (a) Gaussian, (b) rectangular, and (c) Lorentzian. $A_0 = 0.01$ a.u., $\omega_c = 1.00$ a.u., $N_r = 50,000$, $N_{\text{Cheb}} = 2500$, $\gamma = 0.001$ a.u. Note that the data shown here are identical to Fig. 4 except that the intensity is on a log scale.

$\sigma_E$. Initially, at the range of low disorders, $0 < \sigma/\tilde{A}_0 < 2$, the collapse of Rabi splitting is fast, while at large disorders ($2 < \sigma/\tilde{A}_0 < 8$), the collapse is slower. By $\sigma/\tilde{A}_0 = 10$, the UP and LP are indistinguishable from one another, and $\Omega_{\text{R}} \to 0$. At very weak disorder ($0 < \sigma/\tilde{A}_0 < 1$), it is evident that the transmission spectrum is slightly broadened by the presence of the molecular disorder before starting to collapse [29]. This is more evident on the log scale shown in Fig. 3(a) by the broad spectral feature at $\sigma/\tilde{A}_0 = 1.0$. This was also evident in a previous analytical theory exploring such Gaussian-disordered molecular energies [29]. Furthermore,
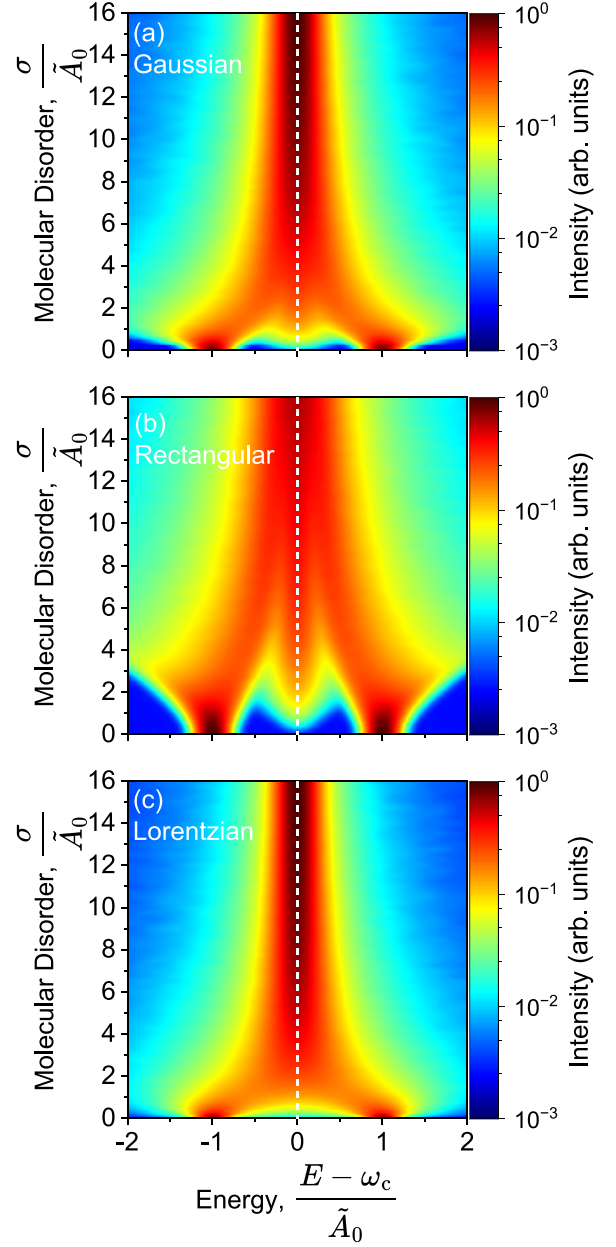
we note that while the two maxima in the transmission spectra corresponding to the UP and LP spectral peaks are collapsing due to the presence of disorder, the edge of the spectra (whose states are composed of mostly matter character due to highly off-resonant molecular energies) continues to spread outward. This can be seen in Fig. 2(a), but is more obviously depicted on a log scale shown in Fig. 3(a). Note that the log intensity exhibits noise due to the stochastic trace in the region of TM = $10^{-2}$–$10^{-3}$ region of intensity.

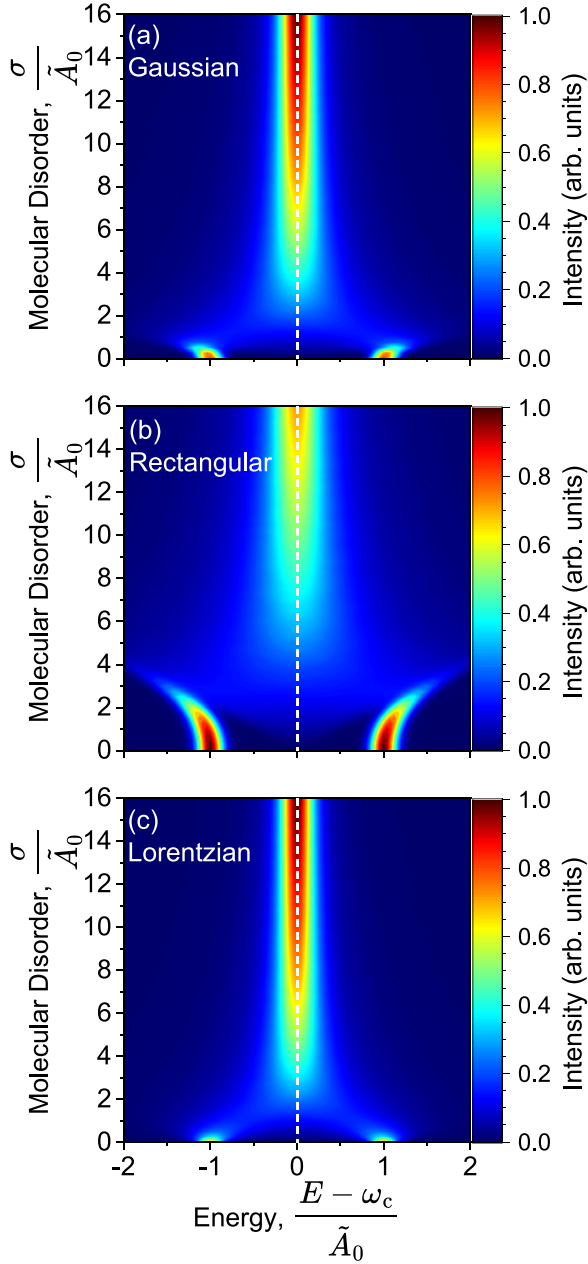For the rectangular distribution for $N = 1$ in Fig. 2(b), we find that the UP and LP spectral peaks converge with

FIG. 6. Transmission spectra for $N = 100$ at varying magnitude of energetic disorders (vertical axis) of the molecules with widths $\sigma$ with distribution (a) Gaussian, (b) rectangular, and (c) Lorentzian. $A_0 = 0.01$ a.u., $\omega_c = 1.00$ a.u., $N_r = 50\,000$, $N_{Cheb} = 2500$, $\gamma = 0.001$ a.u.



FIG. 7. Transmission spectra for $N = 100$ at varying Gaussian energetic disorders (vertical axis) of the molecules with widths $\sigma$ with distribution (a) Gaussian, (b) rectangular, and (c) Lorentzian. $A_0 = 0.01$ a.u., $\omega_c = 1.00$ a.u., $N_r = 50\,000$, $N_{Cheb} = 2500$, $\gamma = 0.001$ a.u. Note that the data shown here are identical to Fig. 6 except that the intensity is on a log scale.

increasing energetic disorder as expected, but the collapse is much slower than for the Gaussian disorder. In fact, the UP and LP states do not fully collapse within 16 $\sigma/\tilde{A}_0$. Most likely, the peaks converge asymptotically as $\sigma/\tilde{A}_0$ increases. We note again that at weak disorder $0 < \sigma/\tilde{A}_0 < 2$, the UP and LP spectral features exhibit a broadening due to the presence of disorder [29]. Furthermore, compared to the Gaussian-disordered case, the initial broadening of the UP and LP spectral bands appears to be slower, as more clearly shown in Figs. 3(a) and 3(b), maximizing the Rabi splitting near $\sigma/\tilde{A}_0 \approx 3$.
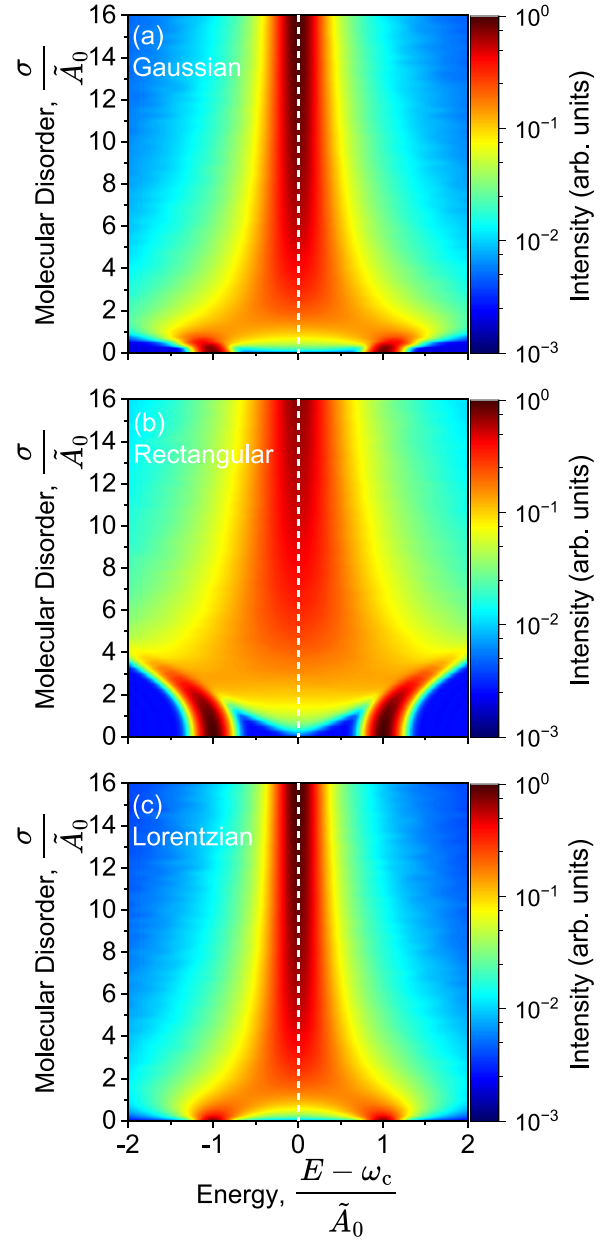
For the last case of Lorentzian distribution for $N = 1$ in Fig. 2(c), the UP and LP collapse is nearly linear in the energy disorder magnitude, while both the Gaussian- and rectangular-disorder cases were nonlinear. Specifically, we are tracking the maximal peak location in the spectra as a function of the disorder. Further, the collapse is much more rapid compared to the other two cases, with LP and UP merging between 2–4 $\sigma/\tilde{A}_0$ compared to more than 16 $\sigma/\tilde{A}_0$ for rectangular and 10 $\sigma/\tilde{A}_0$ for Gaussian. This could be due to the intrinsic long-tailed nature of the Lorentzian distribution compared to the short-tailed Gaussian and no-tail rectangular distributions.
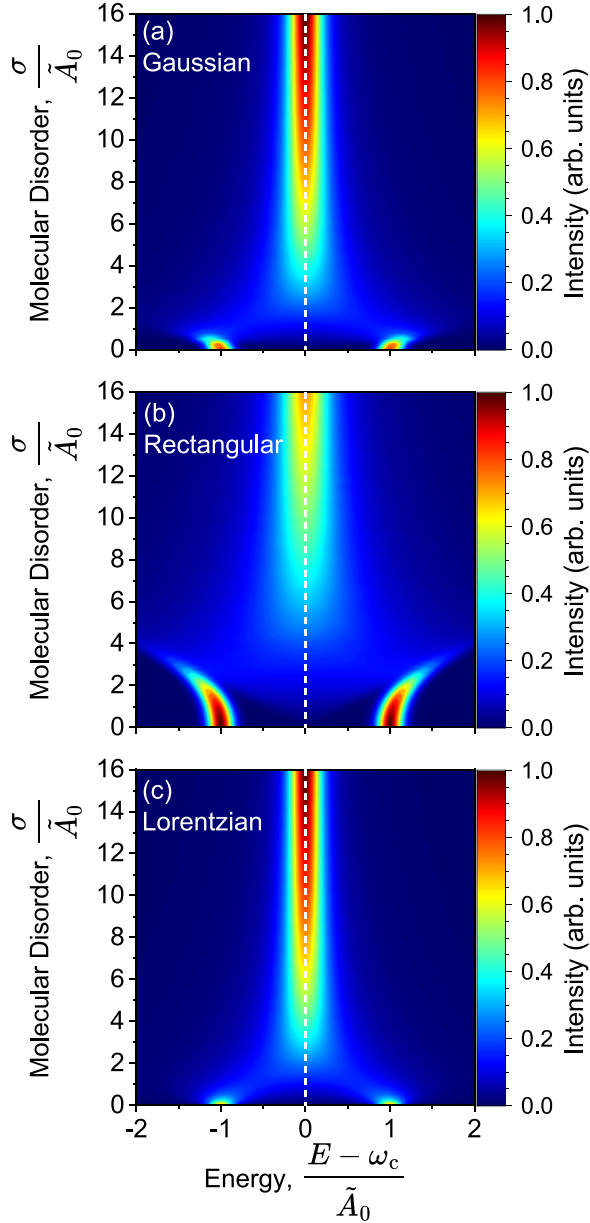
FIG. 8. Transmission spectra for $N = 1000$ at varying magnitude of energetic disorders (vertical axis) of the molecules with widths $\sigma$ with distribution (a) Gaussian, (b) rectangular, and (c) Lorentzian. $A_0 = 0.01$ a.u., $\omega_c = 1.00$ a.u., $N_r = 50\,000$, $N_{\text{Cheb}} = 2500$, $\gamma = 0.001$ a.u.



FIG. 9. Transmission spectra for $N = 1000$ at varying Gaussian energetic disorders (vertical axis) of the molecules with widths $\sigma$ with distribution (a) Gaussian, (b) rectangular, and (c) Lorentzian. $A_0 = 0.01$ a.u., $\omega_c = 1.00$ a.u., $N_r = 50,000$, $N_{\text{Cheb}} = 2500$, $\gamma = 0.001$ a.u. Note that the data shown here are identical to Fig. 8 except that the intensity is on a log scale.

This implies that for few-molecule spectroscopy, for example, in plasmonic cavity designs [11], the emergence of UP and LP spectral features may depend heavily on the shape and magnitude of the molecular disorder. These features of the molecular ensemble are dictated by the internal processes of the molecules as well as by their local environment.

It is important to note that for $N = 1$, there are only two polaritonic states present in the system, the UP and LP, for a given stochastic configuration of the molecular transition energies (one of the $N_r = 50\,000$). Thus, there are no "dark states," even in the absence of molecular disorder. This is evidenced by the lack of transmission intensity in the energy range between the UP and LP spectral bands at any value of
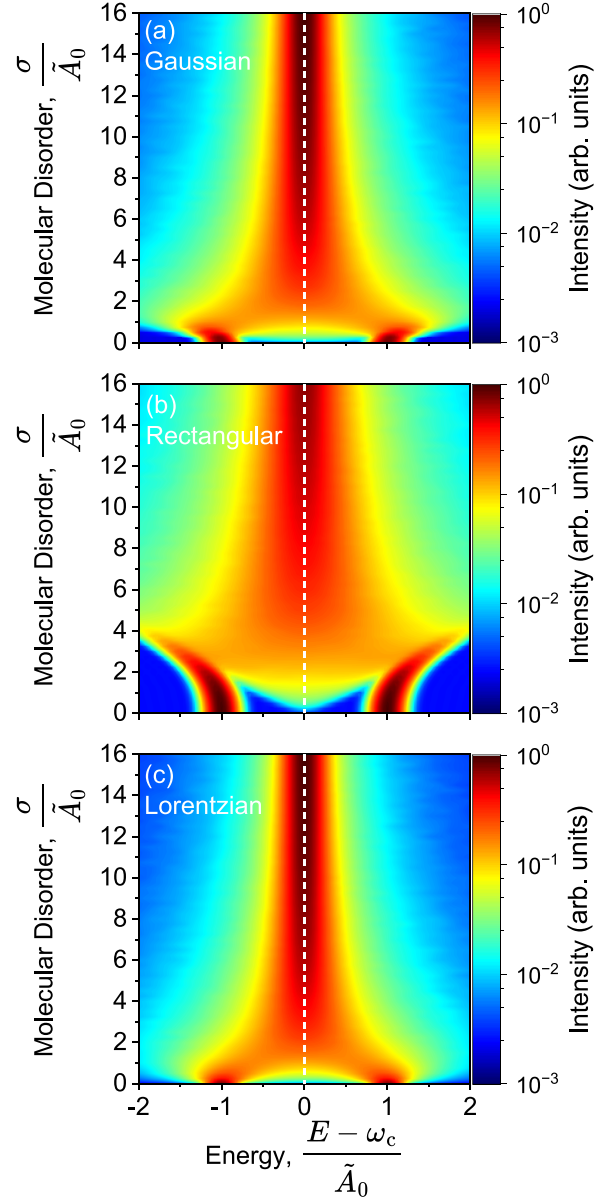
disorder magnitude, most clearly seen in the log-scale rectangular distribution at $E - \omega_c = 0$ [Fig. 3(b), comparing to Fig. 5(b) to be discussed below].

Figure 4 presents similar data as Fig. 2, but now for the case of $N = 2$. In this system, at perfect resonance between the two molecular excitations and the cavity photon excitation and at zero molecular disorder, there is one UP, one LP, and one dark state (i.e., a polaritonic state with no photonic character). At finite molecular disorder, we can immediately recognize the emergence of intermediate/middle polaritonic states within the spectra, hereafter denoted the middle-polariton (MP) spectral feature. This is seen most clearly for the Gaussian

[Fig. 4(a)] and rectangular [Fig. 4(b)] cases which emerges at $\sim 2\,\sigma/\tilde{A}_0$ and $3\,\sigma/\tilde{A}_0$, respectively. This is more evident in the log-scale analogs shown in Figs. 5(a) and 5(b). The Lorentzian case shows little-to-no MP formation since the collapse of the UP and LP peaks occurs rapidly due to the long-tailed distribution.

Notably, for the Gaussian-disordered case with $N = 2$ [Fig. 4(a)], the collapse of the UP and LP peaks becomes much more linear until their collapse at $\sim 4\,\sigma/\tilde{A}_0$ compared to the slower collapse occurring at $10\,\sigma/\tilde{A}_0$ for the single-molecule case [Fig. 2(a)]. Thus, moving from the single-molecule strong coupling to the case of a few-molecule strong coupling, the collapse of the UP and LP spectral features occurs much more rapidly with increasing molecular disorder. This observation can be explained by the fact that the two molecular transitions can both cause a splitting with the photonic DOF, but at a weaker magnitude. Recall that for $N = 2$, the single-molecule coupling strength is scaled down by $1/\sqrt{2}$ to keep a fixed Rabi splitting at zero disorder. Thus, in the presence of disorder, the collapse of the UP and LP features occurs more rapidly due to the weaker single-molecule coupling strength. As such, this effect may already be evidenced by few-molecule plasmonic experiments if the number of molecules can be rigorously constrained to one or a few (2–5) molecules. Additionally, the UP and LP spectral features again exhibit a slight broadening at weak disorder before the collapse.

For the rectangular-disordered case and $N = 2$ [Fig. 4(b)] the emergence of the MP feature (near $3\,\sigma/\tilde{A}_0$) is more evident than in the Gaussian-disordered case [Fig. 4(a)] and retains its identity for a larger range of disorder ($3 < \sigma/\tilde{A}_0 < 9$) than the Gaussian case. Further, the collapse of the UP and LP occurs earlier than for the $N = 1$ case, now at $\sigma/\tilde{A}_0 \sim 14$. The Lorentzian-disordered case, however, shows none of the spectral changes, compared to the Gaussian and rectangular cases, moving from one to two molecules. As we will see, the Lorentzian case has negligible changes for any number of coupled molecules $N$.

Figure 6 presents the data with $N = 100$. For the Gaussian case [Fig. 6(a)], we observe the clearest evidence that at weak disorder, the UP and LP spectral peaks *increase* their Rabi splitting slightly before contracting [29,63]. Of course, as noted before, the eigenstates of the Hamiltonian still increase their overall splitting with increased disorder, but the photonic character becomes energetically localized to the resonance energy once the molecules have become sufficiently dispersed and largely off resonant. Recall that the single-molecule coupling is now scaled down by $1/\sqrt{100}$ compared to the $N = 1$ case (Fig. 2).

Interestingly, the rectangular distribution takes on a completely new character, now exhibiting outward-facing spectral features at lower disorders (i.e., increasing the Rabi splitting when $0 < \sigma/\tilde{A}_0 < 5$). Of the three distributions, the rectangular distribution contains the largest average probability density, $\langle \mathcal{P}^{\mathrm{R}} \rangle_E > \langle \mathcal{P}^{\mathrm{G}} \rangle_E \approx \langle \mathcal{P}^{\mathrm{L}} \rangle_E$ [see Eqs. (16)–(18)]. For the case of $N = 1$ or $N = 2$, we hypothesize that the molecular distribution for a given stochastic configuration cannot well enforce the hard boundaries at $E = \omega_{\mathrm{c}} \pm \frac{\sigma}{2}$, while for $N = 100$, the hard boundaries are evident for most statistical samples in the average, allowing for the formation of

polaritons which also exhibit the features dictated by such hard boundaries. Such features were also discussed in Ref. [29], where the authors analyzed the same excitation frequency distributions using a large-$N$ expansion of the problem and extracting the analytic molecular susceptibility $\chi(E)$. This is also discussed in the recent work using perturbation theory analysis [74] and response-function-based simulations [63] of the linear absorption spectra. Notably, our results at $N = 100$ match the features predicted by the large-$N$ analytical theory in Ref. [29].

We also find that the formation of unique MP features is negligible for the Gaussian and Lorentzian cases in Figs. 7(a) and 7(c). Instead, a broad spectral activation is noted between the UP and LP peaks, nearly equally intense at all points for the Gaussian distribution and slightly curved for the Lorentzian case. This drastically contrasts with the rectangular distribution, which showcases a nearly linear broadening from a point ($E - \omega_{\mathrm{c}} = 0$) for the MP feature as a function of the disorder magnitude (Fig. 7).

In the final case for $N = 1000$ (Figs. 8 and 9), we find nearly identical results as for the $N = 100$ case (Figs. 6 and 7). Thus, interestingly, the collective effects involved in linear transmission spectroscopy inside the cavity are converged with only 100 coupled molecules for the model system considered here. This is likely due to the fact that the dynamics among the collective states are only sensitive to collective quantities, $\sqrt{N}A_0$, as shown in recent theoretical works [64–66]. While the converged simulation requires averaging over a statistical ensemble of molecules, in the experiment, this is automatically accounted for due to time-evolving thermal fluctuations of the molecules.

## VI. CONCLUSIONS

In this work, we use a stochastic-Chebyshev-expansion approach to simulate the linear spectroscopic signatures of exciton polaritons under varying types of molecular frequency disorder: (i) Gaussian, (ii) rectangular, and (iii) Lorentzian. We find that the transmission spectra exhibit drastically varied characteristics between different electronic disorder types as well as, for a fixed type of disorder, between one-, two-, and many-molecule systems. Specifically, for the Gaussian and rectangular disorders, we found that the rate of collapse of the upper and lower polariton spectral features increases with an increasing number of molecules from $N = 1$ to 2. Further, the spectral features at weak disorders are drastically changing with increasing numbers of coupled molecules in both the Gaussian and rectangular disorders. At all numbers of coupled molecules, $N$, both the Gaussian and rectangular disorder types exhibit an increased Rabi splitting at weak disorder prior to its collapse, which agrees with previous analytical work in the large-$N$ limit [29].

Contrary to Gaussian and rectangular disorder, the Lorentzian disorder does not exhibit any changes with increasing numbers of coupled molecules $N$. Additionally, Lorentzian disorder does not exhibit strong middle-polariton formation (i.e., the "brightening" of the dark states due to disorder) compared to other disorder types. The rectangular distribution exhibits the strongest MP formation.

Interestingly, and most importantly, we find that the number of molecules necessary to saturate the collective effects for linear transmission spectroscopy is $N \sim 100$ or less, irrespective of the disorder type and magnitude, as long as the collective-coupling strength $\sqrt{N}A_0$ is kept fixed. We emphasize that this convergence is only with respect to the linear spectroscopic features and not with respect to any dynamical properties such as the nonradiative relaxation between polaritonic states, which depends on the number of molecules (i.e., the number of intermediate polariton states) in the system. Therefore, our results should be considered as the first step in understanding collective effects on linear spectroscopy as a whole. On the other hand, our previous theoretical work [64–66] suggests that if the relaxation are dictated by a "golden rule" type of law, then even the dynamics are largely dictated by the collective quantity $\sqrt{N}A_0$.

In the future, we will extend this exploration in three directions: (i) a nonlinear response via a modification of the observable in Eq. (15), (ii) the inclusion of multimode cavity structures [28], and (iii) dynamical effects through Chebyshev propagation [63,75], all with varied molecular distributions and number of collectively coupled molecules. Further, the inclusion of the dipole self-energy (DSE), while small, may yield nontrivial results in the large-$N$ limit due to the $\propto N$ scaling of the DSE term compared to the $\propto \sqrt{N}$ scaling of the bilinear coupling term.

Thus, it is our hope that these works will give insight into the collective nature of the exciton-polariton systems and provide a sense of intuitive understanding of the number of molecules necessary for the convergence of collective effects. This deeper understanding will help to stimulate future experiments and theoretical studies alike by finding the common ground between the simple single- or few-molecule simulations and, compared to the seemingly difficult single-molecule experiments, many-molecule experiments.

## ACKNOWLEDGMENTS

## DATA AVAILABILITY

The data that support the findings of this article are openly available [72].

[1] F. Pavošević, R. L. Smith, and A. Rubio, Computational study on the catalytic control of endo/exo Diels-Alder reactions by cavity quantum vacuum fluctuations, Nat. Commun. **14**, 2766 (2023).

[2] F. Pavošević, R. L. Smith, and A. Rubio, Cavity click chemistry: Cavity-catalyzed azide-alkyne cycloaddition, J. Phys. Chem. A **127**, 10184 (2023).

[3] B. M. Weight, T. D. Krauss, and P. Huo, Investigating molecular exciton polaritons using *ab initio* cavity quantum electrodynamics, J. Phys. Chem. Lett. **14**, 5901 (2023).

[4] B. M. Weight, D. J. Weix, Z. J. Tonzetich, T. D. Krauss, and P. Huo, Cavity quantum electrodynamics enables para- and ortho-selective electrophilic bromination of nitrobenzene, J. Am. Chem. Soc. **146**, 16184 (2024).

[5] J. Wang, B. M. Weight, and P. Huo, Investigating cavity quantum electrodynamics-enabled endo/exo- selectivities in a Diels-Alder reaction, J. Phys. Chem. A **129**, 5458 (2025).

[6] B. M. Weight, S. Tretiak, and Y. Zhang, Diffusion quantum Monte Carlo approach to the polaritonic ground state, Phys. Rev. A **109**, 032804 (2024).

[7] A. Mandal, M. A. D. Taylor, and P. Huo, Theory for cavity-modified ground-state reactivities via electron-photon interactions, J. Phys. Chem. A **127**, 6830 (2023).

[8] B. M. Weight and P. Huo, *Ab initio* approaches to simulate molecular polaritons: Properties and quantum dynamics, ChemRxiv (2024).

[9] B. M. Weight, X. Li, and Y. Zhang, Theory and modeling of light-matter interactions in chemistry: Current and future, Phys. Chem. Chem. Phys. **25**, 31554 (2023).

[10] J. A. Hutchison, T. Schwartz, C. Genet, E. Devaux, and T. W. Ebbesen, Modifying chemical landscapes by coupling to vacuum fields, Angew. Chem. Int. Ed. **51**, 1592 (2012).

[11] R. Chikkaraddy, B. de Nijs, F. Benz, S. J. Barrow, O. A. Scherman, E. Rosta, A. Demetriadou, P. Fox, O. Hess, and J. J. Baumberg, Single-molecule strong coupling at room temperature in plasmonic nanocavities, Nature (London) **535**, 127 (2016).

[12] A. Dutta, V. Tiainen, I. Sokolovskii, L. Duarte, N. Markešević, D. Morozov, H. A. Qureshi, S. Pikker, G. Groenhof, and J. J. Toppari, Thermal disorder prevents the suppression of ultra-fast photochemistry in the strong light-matter coupling regime, Nat. Commun. **15**, 6600 (2024).

[13] K. Hirai, J. A. Hutchison, and H. Uji-i, Molecular chemistry in cavity strong coupling, Chem. Rev. **123**, 8099 (2023).

[14] D. Hu, B. Chng, W. Ying, and P. Huo, Trajectory-based nonadiabatic simulations of the polariton relaxation dynamics, J. Chem. Phys. **162**, 124113 (2025).

[15] A. Mandal, M. A. D. Taylor, B. M. Weight, E. R. Koessler, X. Li, and P. Huo, Theoretical advances in polariton chemistry and molecular cavity quantum electrodynamics, Chem. Rev. **123**, 9786 (2023).

[16] L. Qiu, A. Mandal, O. Morshed, M. T. Meidenbauer, W. Girten, P. Huo, A. N. Vamivakas, and T. D. Krauss, Molecular polaritons generated from strong coupling between CdSe nanoplatelets and a dielectric optical cavity, J. Phys. Chem. Lett. **12**, 5030 (2021).

[17] A. George, T. Geraghty, Z. Kelsey, S. Mukherjee, G. Davidova, W. Kim, and A. J. Musser, Controlling the manifold of polariton states through molecular disorder, Adv. Opt. Mater. **12**, 2302387 (2024).

[18] T. Khazanov, S. Gunasekaran, A. George, R. Lomlu, S. Mukherjee, and A. J. Musser, Embrace the darkness: An experimental perspective on organic exciton-polaritons, Chem. Phys. Rev. **4**, 041305 (2023).

[19] C. Möhl, A. Graf, F. J. Berger, J. Lüttgens, Y. Zakharko, V. Lumsargis, M. C. Gather, and J. Zaumseil, Trion-polariton formation in single-walled carbon nanotube microcavities, ACS Photonics **5**, 2074 (2018).

[20] A. Graf, M. Held, Y. Zakharko, L. Tropf, M. C. Gather, and J. Zaumseil, Electrical pumping and tuning of exciton-polaritons in carbon nanotube microcavities, Nat. Mater. **16**, 911 (2017).

[21] A. Graf, L. Tropf, Y. Zakharko, J. Zaumseil, and M. C. Gather, Near-infrared exciton-polaritons in strongly coupled single-walled carbon nanotube microcavities, Nat. Commun. **7**, 13078 (2016).

[22] R. H. Tichauer, J. Feist, and G. Groenhof, Multi-scale dynamics simulations of molecular polaritons: The effect of multiple cavity modes on polariton relaxation, J. Chem. Phys. **154**, 104112 (2021).

[23] R. H. Tichauer, D. Morozov, I. Sokolovskii, J. J. Toppari, and G. Groenhof, Identifying vibrations that control non-adiabatic relaxation of polaritons in strongly coupled molecule–cavity systems, J. Phys. Chem. Lett. **13**, 6259 (2022).

[24] G. Groenhof, C. Climent, J. Feist, D. Morozov, and J. J. Toppari, Tracking polariton relaxation with multiscale molecular dynamics simulations, J. Phys. Chem. Lett. **10**, 5476 (2019).

[25] H. L. Luk, J. Feist, J. J. Toppari, and G. Groenhof, Multi-scale molecular dynamics simulations of polaritonic chemistry, J. Chem. Theory Comput. **13**, 4324 (2017).

[26] L. M. A. de Jong, A. M. Berghuis, M. S. Abdelkhalik, T. P. A. van der Pol, M. M. Wienk, R. A. J. Janssen, and J. Gómez Rivas, Enhancement of the internal quantum efficiency in strongly coupled P3HT-$C_{60}$ organic photovoltaic cells using Fabry-Perot cavities with varied cavity confinement, Nanophotonics **13**, 2531 (2024).

[27] G. Lavarda, A. M. Berghuis, K. Joseph, J. J. B. van der Tol, S. Murai, J. Gómez Rivas, and E. W. Meijer, Tunable emission from H-type supramolecular polymers in optical nanocavities, Chem. Commun. **60**, 2812 (2024).

[28] N. C. Bradbury, R. F. Ribeiro, J. R. Caram, and D. Neuhauser, Stochastic methodology shows molecular interactions protect two-dimensional polaritons, Phys. Rev. B **109**, L241303 (2024).

[29] K. Schwennicke, N. C. Giebink, and J. Yuen-Zhou, Extracting accurate light-matter couplings from disordered polaritons, Nanophotonics **13**, 2469 (2024).

[30] D. Sidler, C. Schäfer, M. Ruggenthaler, and A. Rubio, Polaritonic chemistry: Collective strong coupling implies strong local modification of chemical properties, J. Phys. Chem. Lett. **12**, 508 (2021).

[31] M. Amin, E. R. Koessler, O. Morshed, F. Awan, Nicole M. B. Cogan, R. Collison, T. M. Tumiel, W. Girten, C. Leiter, A. N. Vamivakas, P. Huo, and T. D. Krauss, Cavity controlled upconversion in CdSe nanoplatelet polaritons, ACS Nano **18**, 21388 (2024).

[32] O. Morshed, M. Amin, N. M. B. Cogan, E. R. Koessler, R. Collison, T. M. Tumiel, W. Girten, F. Awan, L. Mathis, P. Huo, A. N. Vamivakas, T. W. Odom, and T. D. Krauss, Room-temperature strong coupling between CdSe nanoplatelets and a metal-DBR Fabry-Pérot cavity, J. Chem. Phys. **161**, 014710 (2024).

[33] F. Freire-Fernández, N. G. Sinai, M. J. H. Tan, S.-M. Park, E. R. Koessler, T. Krauss, P. Huo, and T. W. Odom, Room-temperature polariton lasing from CdSe core-only nanoplatelets, ACS Nano **18**, 15177 (2024).

[34] M. E. Mondal, E. R. Koessler, J. Provazza, A. N. Vamivakas, S. T. Cundiff, T. D. Krauss, and P. Huo, Quantum dynamics simulations of the 2D spectroscopy for exciton polaritons, J. Chem. Phys. **159**, 094102 (2023).

[35] R. Pandya, A. Ashoka, K. Georgiou, J. Sung, R. Jayaprakash, S. Renken, L. Gai, Z. Shen, A. Rao, and A. J. Musser, Tuning the coherent propagation of organic exciton-polaritons through dark state delocalization, Adv. Sci. **9**, 2105569 (2022).

[36] R. H. Tichauer, I. Sokolovskii, and G. Groenhof, Tuning the coherent propagation of organic exciton-polaritons through the cavity Q-factor, Adv. Sci. **10**, 2302650 (2023).

[37] A. M. Berghuis, R. H. Tichauer, L. M. A. de Jong, I. Sokolovskii, P. Bai, M. Ramezani, S. Murai, G. Groenhof, and J. Gómez Rivas, Controlling exciton propagation in organic crystals through strong coupling to plasmonic nanoparticle arrays, ACS Photonics **9**, 2263 (2022).

[38] A. M. Berghuis, A. Boom, R. P. Argante, S. Murai, and J. Gómez Rivas, Condensation of exciton-polaritons in a bound state in the continuum: Effects of the excitation spot size and polariton transport, ACS Nano **18**, 31987 (2024).

[39] B. X. K. Chng, M. E. Mondal, W. Ying, and P. Huo, Quantum dynamics simulations of exciton polariton transport, Nano Lett. **25**, 1617 (2025).

[40] W. Ying, B. X. K. Chng, M. Delor, and P. Huo, Microscopic theory of polariton group velocity renormalization, arXiv:2411.08288.

[41] S. R. Koshkaki, A. Manjalingal, L. Blackham, and A. Mandal, Exciton-polariton dynamics in multilayered materials, arXiv:2502.12933.

[42] M. Ruggenthaler, J. Flick, C. Pellegrini, H. Appel, I. V. Tokatly, and A. Rubio, Quantum-electrodynamical density-functional theory: Bridging quantum optics and electronic-structure theory, Phys. Rev. A **90**, 012508 (2014).

[43] J. Flick, M. Ruggenthaler, H. Appel, and A. Rubio, Kohn–Sham approach to quantum electrodynamical density-functional theory: Exact time-dependent effective potentials in real space, Proc. Natl. Acad. Sci. USA **112**, 15285 (2015).

[44] J. Flick, M. Ruggenthaler, H. Appel, and A. Rubio, Atoms and molecules in cavities, from weak to strong coupling in quantum-electrodynamics (QED) chemistry, Proc. Natl. Acad. Sci. USA **114**, 3026 (2017).

[45] J. Flick, D. M. Welakuh, M. Ruggenthaler, H. Appel, and A. Rubio, Light–matter response in nonrelativistic quantum electrodynamics, ACS Photonics **6**, 2757 (2019).

[46] D. S. Wang, C. J. Ciccarino, J. Flick, and P. Narang, Hybridized defects in solid-state materials as artificial molecules, ACS Nano **15**, 5240 (2021).

[47] J. J. Foley, IV, J. F. McTague, and A. E. DePrince, III, *Ab initio* methods for polariton chemistry, Chem. Phys. Rev. **4**, 041301 (2023).

[48] T. Schnappinger, D. Sidler, M. Ruggenthaler, A. Rubio, and M. Kowalewski, Cavity Born-Oppenheimer Hartree-Fock ansatz:

Light-matter properties of strongly coupled molecular ensembles, J. Phys. Chem. Lett. **14**, 8024 (2023).

[49] D. Sidler, M. Ruggenthaler, C. Schäfer, E. Ronca, and A. Rubio, A perspective on *ab initio* modeling of polaritonic chemistry: The role of non-equilibrium effects and quantum collectivity, J. Chem. Phys. **156**, 230901 (2022).

[50] L. Blackham, A. Manjalingal, S. R. Koshkaki, and A. Mandal, Microscopic theory of polaron-polariton dispersion and propagation, arXiv:2501.16622.

[51] A. Mandal, D. Xu, A. Mahajan, J. Lee, M. Delor, and D. R. Reichman, Microscopic theory of multimode polariton dispersion in multilayered materials, Nano Lett. **23**, 4082 (2023).

[52] F. Herrera and F. C. Spano, Cavity-controlled chemistry in molecular ensembles, Phys. Rev. Lett. **116**, 238301 (2016).

[53] F. Herrera and F. C. Spano, Absorption and photoluminescence in organic cavity QED, Phys. Rev. A **95**, 053867 (2017).

[54] G. Engelhardt and J. Cao, Unusual dynamical properties of disordered polaritons in microcavities, Phys. Rev. B **105**, 064205 (2022).

[55] G. Engelhardt and J. Cao, Polariton localization and dispersion properties of disordered quantum emitters in multimode microcavities, Phys. Rev. Lett. **130**, 213602 (2023).

[56] G. D. Scholes, C. A. DelPo, and B. Kudisch, Entropy reorders polariton states, J. Phys. Chem. Lett. **11**, 6389 (2020).

[57] S. Schütz, J. Schachenmayer, D. Hagenmüller, G. K. Brennen, T. Volz, V. Sandoghdar, T. W. Ebbesen, C. Genes, and G. Pupillo, Ensemble-induced strong light-matter coupling of a single quantum emitter, Phys. Rev. Lett. **124**, 113602 (2020).

[58] M. Hertzog, M. Wang, J. Mony, and K. Börjesson, Strong light-matter interactions: A new direction within chemistry, Chem. Soc. Rev. **48**, 937 (2019).

[59] J. Flick and P. Narang, *Ab initio* polaritonic potential-energy surfaces for excited-state nanophotonics and polaritonic chemistry, J. Chem. Phys. **153**, 094116 (2020).

[60] J. Flick and P. Narang, Cavity-correlated electron-nuclear dynamics from first principles, Phys. Rev. Lett. **121**, 113002 (2018).

[61] A. E. DePrince, Cavity-modulated ionization potentials and electron affinities from quantum electrodynamics coupled-cluster theory, J. Chem. Phys. **154**, 094112 (2021).

[62] B. M. Weight and Y. Zhang, Auxiliary field quantum Monte Carlo for electron-photon correlation, arXiv:2505.16021.

[63] M. E. Mondal, A. N. Vamivakas, S. T. Cundiff, T. D. Krauss, and P. Huo, Polariton spectra under the collective coupling regime. I. Efficient simulation of linear spectra and quantum dynamics, J. Chem. Phys. **162**, 014114 (2025).

[64] W. Ying, M. E. Mondal, and P. Huo, Theory and quantum dynamics simulations of exciton-polariton motional narrowing, J. Chem. Phys. **161**, 064105 (2024).

[65] Y. Lai, W. Ying, and P. Huo, Non-equilibrium rate theory for polariton relaxation dynamics, J. Chem. Phys. **161**, 104109 (2024).

[66] B. X. K. Chng, W. Ying, Y. Lai, A. N. Vamivakas, S. T. Cundiff, T. D. Krauss, and P. Huo, Mechanism of molecular polariton decoherence in the collective light–matter couplings regime, J. Phys. Chem. Lett. **15**, 11773 (2024).

[67] T. S. Haugland, E. Ronca, E. F. Kjønstad, A. Rubio, and H. Koch, Coupled cluster theory for molecular polaritons: Changing ground and excited states, Phys. Rev. X **10**, 041043 (2020).

[68] P. Roden and J. J. Foley, IV, Perturbative analysis of the coherent state transformation in *ab initio* cavity quantum electrodynamics, J. Chem. Phys. **161**, 194103 (2024).

[69] S. B. Anantharaman, J. Lynch, M. Aleksich, C. E. Stevens, C. Munley, B. Choi, S. Shenoy, T. Darlington, A. Majumdar, P. J. Schuck, J. R. Hendrickson, J. N. Hohman, and D. Jariwala, Ultrastrong light-matter coupling in two-dimensional metal-organic chalcogenolates, Nat. Photon. **19**, 322 (2025).

[70] M. E. Mondal, A. N. Vamivakas, S. Cundiff, T. Krauss, and P. Huo, Polariton spectra under the collective coupling regime. II. 2D non-linear spectra, J. Chem. Phys. **162**, 074110 (2025).

[71] N. C. Bradbury, C. Chuang, A. P. Deshmukh, E. Rabani, R. Baer, J. R. Caram, and D. Neuhauser, Stochastically realized observables for excitonic molecular aggregates, J. Phys. Chem. A **124**, 10111 (2020).

[72] B. M. Weight and P. Huo, Stochastic Chebyshev, GitHub (2024), https://github.com/bradenmweight/Stochastic_Chebyshev.

[73] A. Hazarika, A. Layek, S. De, A. Nag, S. Debnath, P. Mahadevan, A. Chowdhury, and D. D. Sarma, Ultranarrow and widely tunable $Mn^{2+}$-induced photoluminescence from single Mn-doped nanocrystals of ZnS-CdS alloys, Phys. Rev. Lett. **110**, 267401 (2013).

[74] Z. Zhou, H.-T. Chen, J. E. Subotnik, and A. Nitzan, Interplay between disorder, local relaxation, and collective behavior for an ensemble of emitters outside versus inside a cavity, Phys. Rev. A **108**, 023708 (2023).

[75] D. J. Tannor, *Introduction to Quantum Mechanics: A Time-Dependent Perspective* (University Science Books, Sausalito, CA, 2007).